Modeling the Partial Oxidation of Methane in a Fixed Bed with Detailed Chemistry

M. Bizzi and G. Saracco
Dept. of Materials Science and Chemical Engineering, Politecnico di Torino, 10129 Torino (TO), Italy

R. Schwiedernoch and O. Deutschmann
Institute for Chemical Technology, University of Karlsruhe, Karslruhe, Germany

DOI 10.1002/aic.10118
Published online in Wiley InterScience (www.interscience.wiley.com).

This work presents a model of a fixed-bed reactor for the catalytic partial oxidation of methane to synthesis gas at short contact time. The transient model, one dimensional in space, accounts for separate energy equations for the gas and solid phases, interphase heat and mass transfer, internal radiation within the fixed bed, longitudinal gas-phase dispersion, and detailed surface kinetics. The model is used to analyze the influence of the feedstock composition and temperature on the conversion and selectivity reactor performance. Furthermore, the study also investigates the blowout of the reaction and the impact of reactor geometry on the performance. Reactor scale-up is discussed and a general criterion is formulated. © 2004 American Institute of Chemical Engineers *AIChE J,* 50: 1289–1299, 2004

Keywords: reactor modeling, short contact time catalytic partial oxidation, natural gas, synthesis gas, hydrogen

Introduction

Synthesis gas is a very interesting intermediate product in the chemical industry used for a variety of important processes such as ammonia and methanol synthesis. Nowadays, increasing efforts are devoted to the development of efficient technologies to exploit the existing resources of natural gas. For instance, the development of a reforming unit for the conversion of natural gas to synthesis gas, which subsequently can be fed to a GTL (gas to liquid) process as the Fischer–Tropsch synthesis, is currently of great interest. The liquid fuel then can be more easily transported through the existing oil pipelines, avoiding other more expensive routes for directly transferring the natural gas to the market.

The autothermal partial oxidation of methane, the main component of natural gas, at short contact times shows a great potential for synthesis gas (syngas) production compared to existing technologies. One of the main advantages of this process is an easily set up fixed-bed system running with air instead of pure oxygen, which in many cases is a limiting feature of autothermal systems. Furthermore, the outstanding performance in terms of conversion and products selectivity makes this process even more appealing. Still some technical problems exist to make the process viable at the industrial scale. Despite the use of air as a source of oxygen, which could be on the one hand a considerable advantage in terms of process economics—avoiding the cost of pure oxygen separation—it has to be pointed out that the reaction products would not be clean. From this viewpoint, for several process applications the implementation of a separation section appears unavoidable, thus causing one great potential of this process to vanish. Moreover, it has to be considered that the syngas processes normally operate at high pressures. Thus, the oxidant stream introduced in the catalytic system needs to be compressed, and the energy requirements for the additional compression of the inert nitrogen in air would burden the economics of the short contact time partial oxidation process. Finally, it has been observed in practice and demonstrated in theory

Correspondence concerning this article should be addressed to G. Saracco at guido.saracco@polito.it.

(Bizzi et al., 2003) that higher catalyst temperatures favor the reactor performance, and the use of air could also have detrimental effects from this standpoint. Therefore, as far as the use of pure oxygen or air is concerned, the decision has to be taken on a case-by-case basis, considering quantitatively all these conflicting aspects of the novel process. Finally, some safety issues may arise from the necessity of preheating the feedstock, which has been observed to be a very important lever in the productivity improvement. Unfortunately, this could determine gas-phase preignition of the reactants and the occurrence of "flashback," thus generating serious safety problems. Considering all these aspects the development of a reliable and competitive technology seems to be a challenging task. Nonetheless, the significant market opportunities for efficient syngas and hydrogen production constitute a considerable driving force to achieve this target.

In this article, we describe an efficient predictive mathematical model of a fixed-bed reactor for catalytic partial oxidation of methane operated at short contact times. The numerical simulation based on that model offers a powerful tool that can assist in reactor design and scale-up of the process, thus saving expensive pilot work (Rostrup-Nielsen, 2000). Experimental studies (Hohn and Schmidt, 2001) showed that fixed-bed reactors offer superior performance over that of monoliths, which have been used at an early stage of the lab experiments. The reactor modeled here is that of a fixed-bed reactor with rhodium-coated alumina particles. In our previous work (Bizzi et al., 2003), we carried out a reactor simulation assuming a local thermodynamic equilibrium condition as an approximation for the catalyst reactivity. This simple assumption led to acceptable agreement with the experiments. However, simulations carried out at very high space velocities produced questionable results. Very high space velocities can lead to blowout of the reactor, and their reliable description is therefore significant in reactor scale-up. Considering the importance and the interest in using the model, also out of the range customarily accessible by the experiments, we upgraded our previous work by introducing a more complex, multistep surface kinetic model for the rhodium catalyst.

The model analysis presented in this article was carried out according to the following steps:

- *Model validation.* First, the surface kinetic model used in this study was validated using a set of experimental data minimizing effects other than kinetics (Beretta et al., 1999). Then the predictive behavior of the overall reactor model was assessed by making a comparison with a set of experiments in the literature (Bizzi et al., 2003; Hohn and Schmidt, 2001), reproducing operating conditions typical of industrial runs.
- *Effect of the space velocity and reactor blowout.* Once validated, the model was used to investigate the region of very high space velocities by simulating reactor blowout, which has been hardly observed in practice. This analysis helps to understand the practical limits of gas-hourly space velocity (GHSV) for use in industrial operation, and the benefits/disadvantages arising from increasing the mass flow rate over the "traditional" limits.
- *Effect of the feedstock composition and temperature.* The model was used to investigate the effects of the operating conditions on the reactor performance. The variables considered have been the feedstock mass flow rate (GHSV), composition, and temperature.
- *Reactor geometry.* The analysis focused then on the effects of the reactor geometry on the system stability and performance. Considering the typical cylindrical reactor shape, the diameter-to-length ratio was varied at constant reactor volume, observing conversion and selectivity.
- *Reactor scale-up.* Obviously, at this stage of the work, it is not possible to define unequivocally a criterion for reactor scale-up, which is undoubtedly dependent on economic considerations. However, two basically different guidelines are highlighted, which can define the criteria for operation.

Model Equations

Conservation equations

The model consists of one-dimensional transient equations for mass and energy conservation, which was described in more detail in our previous article (Bizzi et al., 2003).

Gas-Phase Mass Balance

$$S\varepsilon \frac{\partial(\rho_g Y_k)}{\partial t} + \dot{m} \frac{\partial Y_k}{\partial z} + \frac{\partial(V_k S \varepsilon \rho_g Y_k)}{\partial z} + J_k M_k a S = 0 \qquad k = 1, N \quad (1)$$

Gas-Phase Energy Balance

$$S\varepsilon \hat{c}_{pg} \frac{\partial(\rho_g T_g)}{\partial t} + \dot{m} \hat{c}_{pg} \frac{\partial T_g}{\partial z} + \frac{\partial}{\partial z}\left(-k_g S \frac{\partial T_g}{\partial z}\right) + hS(T_g - T_s) = 0 \quad (2)$$

Solid-Phase Energy Balance

$$S(1-\varepsilon)\rho_s \hat{c}_{ps} \frac{\partial T_s}{\partial t} + \frac{\partial}{\partial z}\left(-k_{s,eff} S \frac{\partial T_s}{\partial z}\right) = \sum_k J_k a M_k \hat{H}_k S + hS(T_g - T_s) - \sigma e_r (T_s^4 - T_{room}^4)\pi d_r \quad (3)$$

Ideal Gas Law

$$\rho_g = \frac{p M_g}{R T_g} \quad (4)$$

The diffusive terms in the species conservation equations can be neglected, according to a plug flow assumption, as discussed in Bizzi et al. (2003). The Peclet number of approximately 500 shows that the system operates in a range of space velocities where the longitudinal diffusive mass transfer is unimportant. Gas-phase reactions were neglected because they are not significant at atmospheric pressure (Deutschmann and Schmidt, 1998).

Thermal conduction and radiation within the porous medium were accounted for by an effective thermal conductivity (Bizzi et al., 2003). The solid-phase energy balance takes into account nonadiabatic conditions by means of the reactor emissivity e_r. Energy dispersion is actually not negligible in the experiments (Bizzi et al., 2002, 2003), given that the temperature measurement by IR thermography required that the reactor was not insulated. The wall emissivity value used in the simulation of

those experiments was 0.9, which is a typical value for a quartz material (Perry and Green, 1997). On the other hand, in the simulations of experimental data by Hohn and Schmidt (2001) the wall emissivity has been set to zero, which corresponds to adiabatic conditions.

Boundary conditions

Fixed compositions and gas-phase temperature were specified at the domain inlet and zero-gradient profiles for these variables were set at the outlet. For the solid-phase thermal balance equation, a radiation boundary condition was imposed at both the inlet (Eq. 5) and the outlet (Eq. 6) of the computational domain

$$-k_{s,eff}\left.\frac{\partial T_s}{\partial z}\right|_{z=0} = \sigma e_s(T_{room}^4 - T_s^4|_{z-0}) \tag{5}$$

$$-k_{s,eff}\left.\frac{\partial T_s}{\partial z}\right|_{z=L} = \sigma e_s(T_s^4|_{z=L} - T_{room}^4) \tag{6}$$

Catalyst reactivity

The chemical reactivity of the catalyst was described by means of a multistep surface kinetic model (Deutschmann et al., 2001; Schwiedernoch et al., 2003). The model consists of 38 reactions among six gas-phase species and a further 11 adsorbed species and is suitable for partial and complete oxidation of methane on a rhodium surface. Reactions and kinetic parameters are summarized in Table 1. A sensitivity analysis could perhaps help to reduce the size of the model. However, this goal was out of the scope of the present work and it could be the ground for future model improvements.

The state of the surface is described by its temperature and by a set of surface coverage fractions θ_i. The chemical source term (Deutschmann and Schmidt, 1998) is given as

$$R_k = \sum_{i=1}^{N_r} \nu_{k,i} k_{f,i} \prod_{j=1}^{N} X^{\eta'_{j,i}} \tag{7}$$

The rate coefficients are modeled by a modified Arrhenius equation, as follows

$$k_{f,i} = A_i T^{\beta,i} \exp\left(-\frac{E_{a,i}}{RT}\right) \prod_{j=1}^{N_s} \Theta_i^{\xi_{j,i}} \exp\left(\frac{\xi_{j,i}\Theta_i}{RT}\right) \tag{8}$$

The numerical implementation of the surface kinetic model is based on the software package DETCHEM (Deutschmann), that allows calculation of the coverage fractions at the local conditions of the surface, assuming a quasi steady-state condition on the catalyst, with no species accumulation on the active sites. The experiments in the literature and theoretical calculations (Bizzi et al., 2002) showed that the system operates in a transport-controlled regime. Therefore, the mass-transfer coefficients have to be accounted for in the model, and for this purpose literature expressions have been used (Yoshida et al., 1962)

Table 1. Surface Reaction Mechanism*

Reaction	Kinetic Parameters A	Kinetic Parameters E_a
(1) H_2 + 2Rh(s) ⇒ 2H(s)	1.00×10^{-2}	s.c.
(2) O_2 + 2Rh(s) ⇒ 2O(s)	1.00×10^{-2}	s.c.
(3) CH_4 + Rh(s) ⇒ CH_4(s)	8.00×10^{-3}	s.c.
(4) H_2O + Rh(s) ⇒ H_2O(s)	1.00×10^{-1}	s.c.
(5) CO_2 + Rh(s) ⇒ CO_2(s)	1.00×10^{-5}	s.c.
(6) CO + Rh(s) ⇒ CO(s)	5.00×10^{-1}	s.c.
(7) 2H(s) ⇒ 2Rh(s) + H_2	$3.00 \times 10^{+21}$	77.8
(8) 2O(s) ⇒ 2Rh(s) + O_2	$1.30 \times 10^{+22}$	355.2
(9) H_2O(s) ⇒ H_2O + Rh(s)	$3.00 \times 10^{+13}$	45.0
(10) CO(s) ⇒ CO + Rh(s)	$3.50 \times 10^{+13}$	133.4
(11) CO_2(s) ⇒ CO_2 + Rh(s)	$1.00 \times 10^{+13}$	21.7
(12) CH_4(s) ⇒ CH_4 + Rh(s)	$1.00 \times 10^{+13}$	25.1
(13) O(s) + H(s) ⇒ OH(s) + Rh(s)	$5.00 \times 10^{+22}$	83.7
(14) OH(s) + Rh(s) ⇒ O(s) + H(s)	$3.00 \times 10^{+20}$	37.7
(15) H(s) + OH(s) ⇒ H_2O(s) + Rh(s)	$3.00 \times 10^{+20}$	33.5
(16) Rh(s) + H_2O(s) ⇒ H(s) + OH(s)	$5.00 \times 10^{+22}$	106.4
(17) OH(s) + OH(s) ⇒ H_2O(s) + O(s)	$3.00 \times 10^{+21}$	100.8
(18) O(s) + H_2O(s) ⇒ OH(s) + OH(s)	$3.00 \times 10^{+21}$	224.2
(19) C(s) + O(s) ⇒ CO(s) + Rh(s)	$3.00 \times 10^{+22}$	97.9
(20) CO(s) + Rh(s) ⇒ C(s) + O(s)	$2.50 \times 10^{+21}$	169.0
(21) CO(s) + O(s) ⇒ CO_2(s) + Rh(s)	$1.40 \times 10^{+20}$	121.6
(22) CO_2(s) + Rh(s) ⇒ CO(s) + O(s)	$3.00 \times 10^{+21}$	115.3
(23) CH_4(s) + Rh(s) ⇒ CH_3(s) + H(s)	$3.70 \times 10^{+21}$	61.0
(24) CH_3(s) + H(s) ⇒ CH_4(s) + Rh(s)	$3.70 \times 10^{+21}$	51.0
(25) CH_3(s) + Rh(s) ⇒ CH_2(s) + H(s)	$3.70 \times 10^{+24}$	103.0
(26) CH_2(s) + H(s) ⇒ CH_3(s) + Rh(s)	$3.70 \times 10^{+21}$	44.0
(27) CH_2(s) + Rh(s) ⇒ CH(s) + H(s)	$3.70 \times 10^{+24}$	100.0
(28) CH(s) + H(s) ⇒ CH_2(s) + Rh(s)	$3.70 \times 10^{+21}$	68.0
(29) CH(s) + Rh(s) ⇒ C(s) + H(s)	$3.70 \times 10^{+21}$	21.0
(30) C(s) + H(s) ⇒ CH(s) + Rh(s)	$3.70 \times 10^{+21}$	172.8
(31) CH_4(s) + O(s) ⇒ CH_3(s) + OH(s)	$1.70 \times 10^{+24}$	80.3
(32) CH_3(s) + OH(s) ⇒ CH_4(s) + O(s)	$3.70 \times 10^{+21}$	24.3
(33) CH_3(s) + O(s) ⇒ CH_2(s) + OH(s)	$3.70 \times 10^{+24}$	120.3
(34) CH_2(s) + OH(s) ⇒ CH_3(s) + O(s)	$3.70 \times 10^{+21}$	15.1
(35) CH_2(s) + O(s) ⇒ CH(s) + OH(s)	$3.70 \times 10^{+24}$	158.4
(36) CH(s) + OH(s) ⇒ CH_2(s) + O(s)	$3.70 \times 10^{+21}$	36.8
(37) CH(s) + O(s) ⇒ C(s) + OH(s)	$3.70 \times 10^{+21}$	30.1
(38) C(s) + OH(s) ⇒ CH(s) + O(s)	$3.70 \times 10^{+21}$	145.5

*The units of A are given in terms of [mol, cm, s] and of E_a in [kJ/mol]; s.c. = initial sticking coefficient. The mechanism is given in DETCHEM format; its electronic version, in DETCHEM and CHEMKIN format, can be downloaded from http://www.detchem.com.

$$\begin{cases} J_d = 0.91\ \mathrm{Re}^{-0.51}\psi & 0.01 < \mathrm{Re} < 50 \quad \text{(a)} \\ J_d = 0.61\ \mathrm{Re}^{-0.41}\psi & 50 < \mathrm{Re} < 1000 \quad \text{(b)} \end{cases} \tag{9}$$

with the Reynolds number (Re)

$$\mathrm{Re} = \frac{Gd_p}{6\mu_g(1-\varepsilon)} \tag{10}$$

The diameter of particles used in the simulations is 1.4 mm, unless otherwise specified, and the porosity has been assumed to be 50%. When different particles diameters have been used, the porosity has been varied accordingly, as indicated in Hohn and Schmidt (2001). The same equations were used to calculate the heat transfer coefficients within the fixed bed, according to the Chilton–Colburn analogy (Chilton and Colburn, 1934).

Once the chemical reaction rates and the transport terms have been calculated, the resulting overall source term for each species along the reactor can be easily calculated by considering these phenomena in series. For each species, an equivalent first-order kinetic constant κ_{kin} is calculated by dividing the

chemical source term given in Eq. 7 by its bulk molar concentration. Then, the mass transport coefficient κ_{tr} is determined from Eq. 9. The overall source term for each species is then given as

$$J_k = \left(\frac{1}{\kappa_{kin}} + \frac{1}{\kappa_{tr} a} \right)^{-1} c_k \tag{11}$$

Numerical implementation of the model

A crucial point in our study was the implementation of the surface kinetic model in an appropriate simulation code. The considerable number of simulations necessary to further enlighten the system's behavior pointed out the importance of computation times. Therefore, an approach based on appropriate look-up tables was used to speed up the simulations, avoiding the direct integration of the conservation equations for the surface coverage fractions (Deutschmann and Schmidt, 1998). The simulation code implemented the method of lines, which allowed the reduction of the partial differential equation problem to an initial-value ordinary differential equation problem. The model equations were therefore solved using the initial value integrator LSODES [Livermore Solver for Ordinary Differential Equations (Sherman)] suitable for sparse systems of ODEs (ordinary differential equations) (Hindmarsch, 1983).

Results and Discussion

Kinetic model validation

The first step of the analysis was the validation of the surface intrinsic kinetic mechanism used in this work. It is well known that this can be an extremely challenging task, given the difficulty of performing reactivity experiments under a pure kinetic control regime: this requirement could be difficult or even impossible to be fulfilled especially for very fast reactions, as discussed in Beretta et al. (1999).

The data set used for the validation is the one reported in Beretta et al. (1999) for methane partial oxidation over a rhodium (Rh) catalyst at high GHSV. The experiments were carried out in appropriate operating conditions so as to minimize effects other than kinetics affecting the final conversion and yields. For this purpose, a diluted feedstock was used in a diluted fixed bed consisting of small catalyst particles (~90 microns in diameter) mixed with quartz beads of the same size. The reactor used in the experiments was represented as an isothermal solid-gas plug flow reactor in a pure kinetic control regime. The input data of the reactor model were set according to the experimental details reported in Beretta et al. (1999). The specific area of the catalyst sample was assumed to be 10 m^2/g, which is a reasonable value suggested by experimental practice. The catalyst loading used in the kinetic model validation is 50 mg, as indicated in the referenced experiments; this value was increased to 0.9 g in the following sections according to the details reported in Bizzi et al. (2002). Finally, the site density of Rh in the mechanism is assumed to be 2.72×10^{-9} mol/cm^2. However, the total active catalytic surface area in the current experiment may deviate from that used for the establishment of the mechanism based on monolithic structures. Because we had no experimental possibility for an estimation of this area, the total active catalytic surface was chosen as the fitting parameter to minimize the deviation between model and experiments, according to a least-squares procedure. It was estimated that the total active surface area in the current experiment, using a fixed-bed reactor, is three times larger. This assumption was then used in the rest of the study.

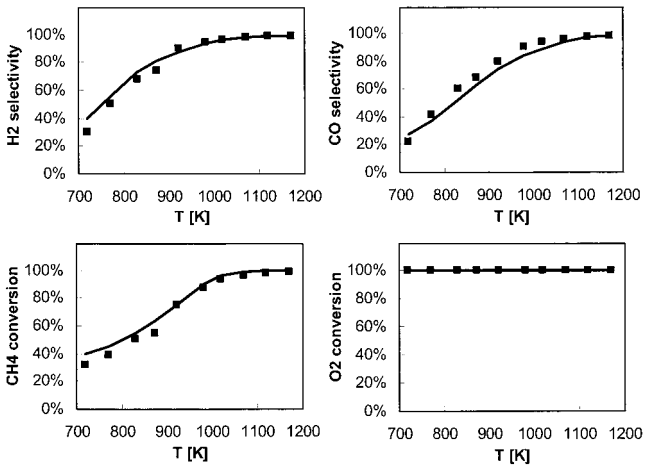

Figure 1. Conversion and selectivity vs. temperature.

Comparison between experiments (Beretta et al., 1999) and calculations performed with the surface model in Table 1.

The comparison between experiments and model calculations is shown in Figure 1, revealing that the model acceptably reproduces methane and oxygen conversions in the whole temperature range under investigation. The hydrogen selectivity is also reproduced satisfactorily, whereas the CO selectivity is slightly underestimated at the lower temperatures considered. In general it could be observed that conversions are slightly underestimated by the model. This is explained, in particular, by the fact that the experiments still suffer from transport limitations because of the extremely fast reactions, as discussed in the following paragraph.

A further analysis of experimental data was performed to define quantitatively the importance of transport phenomena on the methane reactivity at short contact time, and the Mears' criterion was used to measure the importance of external mass transfer (Fogler, 2000). The literature (Fogler, 2000) reports that external mass transfer limitations can be considered negligible below Mears' factor values of 0.15, whereas it can be considered a full transport controlled regime above 15. The operating conditions of the experiments performed by Beretta et al. (1999) allow calculation of a value of the Mears' factor around 0.7, indicating that external mass transfer phenomena still play a role in the overall conversion process but that the system does not operate in a transport-controlled regime. On the other hand, at the typical operating conditions of the industrial reactors, reproduced also in the experiments used in the next sections of this article (Bizzi et al., 2002; Hohn and Schmidt, 2001), the mass transfer limitations are enhanced because of the use of larger catalyst particles, thus giving lower geometrical surface area and lower mass transfer coefficients, and because of the use of an undiluted catalyst bed. The calculated Mears' factor is around 100, thus confirming that the system operates in a transport-controlled regime, as already demonstrated by the authors in a previous article (Bizzi et al., 2002).

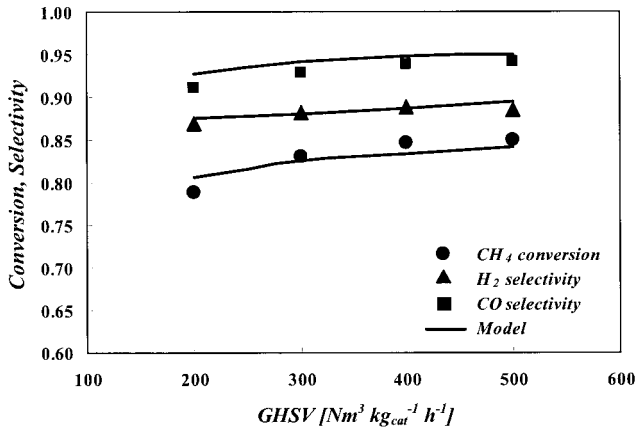

Figure 2. Conversion and selectivity vs. space velocity.

A comparison between model calculations and experiments reported in Bizzi et al. (2002, 2003). Inlet composition $O_2/CH_4/N_2$ = 1.00/2.00/0.43 mol/mol.

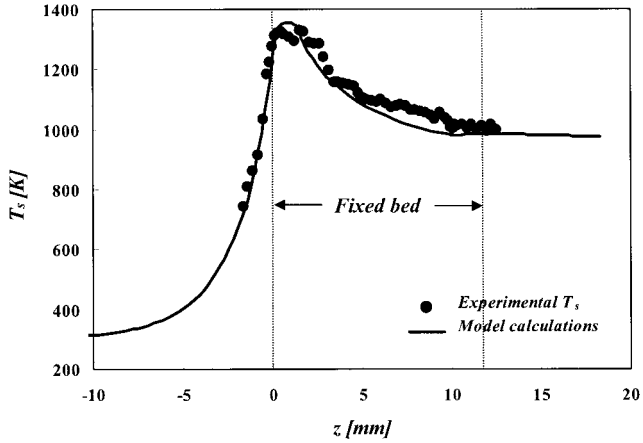

Figure 4. Solid-phase thermal profile measured at GHSV = 3 × 10⁵ $Nm^3\ kg_{cat}^{-1}\ h^{-1}$.

Comparison between experiments and calculations Bizzi et al. (2002, 2003). Inlet composition $O_2/CH_4/N_2$ = 1.00/2.00/0.43 mol/mol.

Reactor model validation

The next step was to set up a comparison between the predictions of the overall reactor model and the existing experimental data on catalytic partial oxidation at short contact times in fixed-bed reactors, operating at conditions closer to industrial practice (Figures 2–5). Figure 2 shows the dependency of conversion and selectivity on space velocity reported in Bizzi et al. (2002, 2003), together with the model calculations. The figure shows that conversion and selectivity increase as GHSV is increased. In the reference experiments, the thermal profiles were measured at different space velocities by an infrared (IR)–thermography technique. Therefore the maximum temperature of the solid phase is also available, as represented in Figure 3. On the same plot, the values of outlet gas temperatures, measured by thermocouples, are reported. The dependency of temperature on space velocity can also be deduced from Figure 3. As the space velocity increases, the conversion increases and the reactor temperature increases concomitantly. Finally, Figure 4 represents a thermal profile along the fixed-bed reactor, measured at GHSV = 300,000 $Nm^3\ kg_{cat}^{-1}\ h^{-1}$. The thermal profile exhibits a peak corresponding to the completion of exothermic oxidation reactions. The then decreasing profile is attributed not only to heat conduction toward the reactor outlet but also to the endothermic steam-reforming reaction occurring.

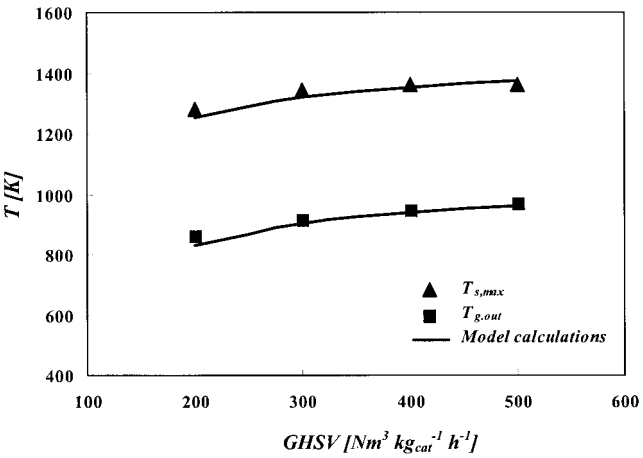

Figure 3. Maximum catalyst temperature and outlet gas temperature vs. space velocity.

A comparison between model calculations and experiments reported in Bizzi et al. (2002, 2003).
Inlet composition $O_2/CH_4/N_2$ = 1.00/2.00/0.43 mol/mol.

All the figures reveal a rather good agreement between the experiments and the calculated values. The typical features of catalytic partial oxidation at short contact times are observed. As the space velocity increases, methane conversion increases together with the selectivity of the products. This can be explained by assuming that the reaction rate is enhanced by the mass flow rate because at higher GHSV, despite a reduction of the residence time, an increase in the syngas selectivity is observed. Intrinsic kinetics is not influenced by the mass flow rate. Then it can be concluded that the system operates under a transport-controlled regime. Increased methane conversion then determines a higher energy input in the solid phase and therefore higher temperatures, which favor synthesis gas production.

Finally, Figure 5 illustrates the comparison between the calculations performed by the present model and experimental data reported in Hohn and Schmidt (2001), for two different values of particle size. The agreement between the model and the experiments is also reasonable in this case. The model clearly overestimates measured methane conversion in the case of the smaller diameter, and underestimates experiments with the larger one. This indicates that the model is perhaps more sensitive than necessary to the change in the mass-transfer features related to the variation of the particles' dimension.

A comparison between Figures 2 and 5 reveals that the performance improvements achieved at higher GHSV is more pronounced in the case of the nonadiabatic system. This observation could be explained by considering that higher GHSVs determine higher energy inputs inside the system. This effect prevails over the enhancement of the nonadiabatic thermal dispersion toward the environment, occurring as GHSV is increased. The increase in input energy occurring as GHSV

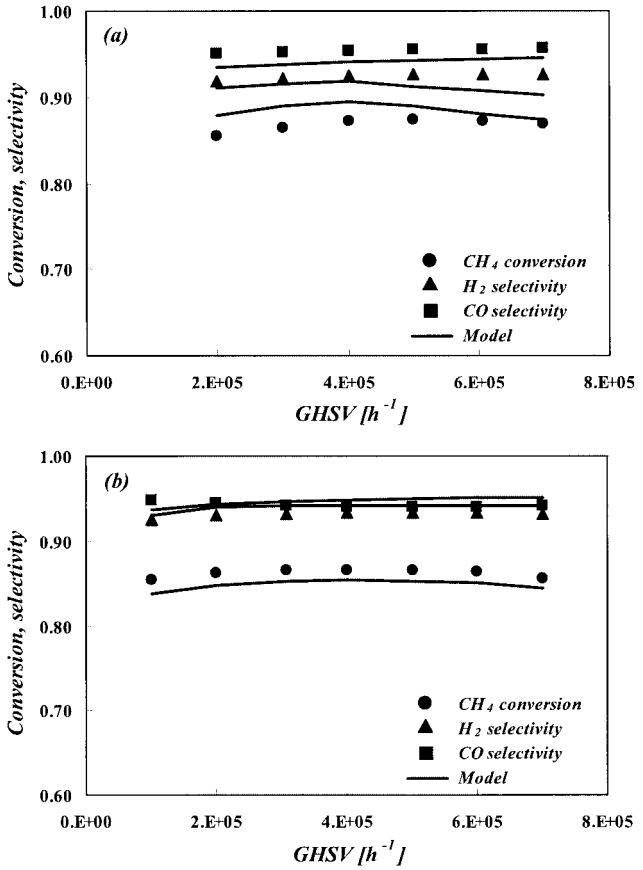

Figure 5. Conversion and selectivity vs. space velocity.

A comparison between model calculations and experiments reported in Hohn and Schmidt (2001): (a) $d_p = 0.4$ mm; (b) $d_p = 0.8$ mm.

increases has a steeper slope than the average solid phase temperature increase, as calculated in Bizzi et al. (2003). As a result, the fraction of the input energy retained in the system increases with GHSV, thus reducing the nonadiabatic behavior of the reactor at higher space velocities. For this reason, the nonadiabatic system appears more sensitive to GHSV than the perfectly insulated one.

Effect of the space velocity and reactor blowout

Once it has been validated, the model was then used to study the system behavior near blowout conditions. The analysis of blowout is of considerable importance in practice. The maximum productivity of an industrial unit (that is, mass of syngas produced per unit time per unit reactor volume) would be in fact obtained at those operating conditions where high conversion and selectivity are preserved and where the maximum flow rate is processed. However, a trade-off condition will exist between maximum productivity and compression energy demand to define the optimal operating conditions, given that pressure drop will increase with flow rate. The investigation of the reactor behavior at the "physical" limits of the system operation is necessary to deal with these considerations.

Figure 6 reports the results obtained by varying the mass flow rate by several orders of magnitude, to span a space velocity interval between 2×10^4 and 3×10^7 h^{-1}. The numerically predicted methane conversion [Figure 6a] reveals that, at low space velocities, the increment in mass flow rate determines an increase in the system performance that can be ascribed to the improvement in the transfer coefficients, which depend on the Reynolds number, as stated by Eq. 9. Despite this effect, the CH_4 conversion decreases at higher space velocities. In this case, the reduction in contact time prevails over the beneficial effect of the increment of transfer coefficients. Together with CH_4 conversion, the H_2 selectivity decreases as well. According to the surface model used, the formation of H_2 is largely provided by the steam-reforming reaction, which follows the initial formation of CO and H_2O by direct oxidation. As the residence time decreases, this reaction is not completed and therefore the reduction in the conversion of methane and a decrease in H_2 selectivity (GHSV $< 10^6$ h^{-1}) are observed. A further residence time reduction also determines a decrease in the O_2 conversion (GHSV $= 10^6$–10^7 h^{-1}). Particular attention must be devoted to CO. Its selectivity does not decrease during blowout according to our simulations. This is attributed to the surface reaction mechanism applied, which states a direct formation of CO out of CH_4 oxidation. Moreover, CO selectivity increases with temperature, according to the model. As discussed in detail later, the system temperatures increase with space velocity, further promoting CO over CO_2. These considerations explain the slightly increasing trend in CO selectivity that can be observed in the calculations pre-

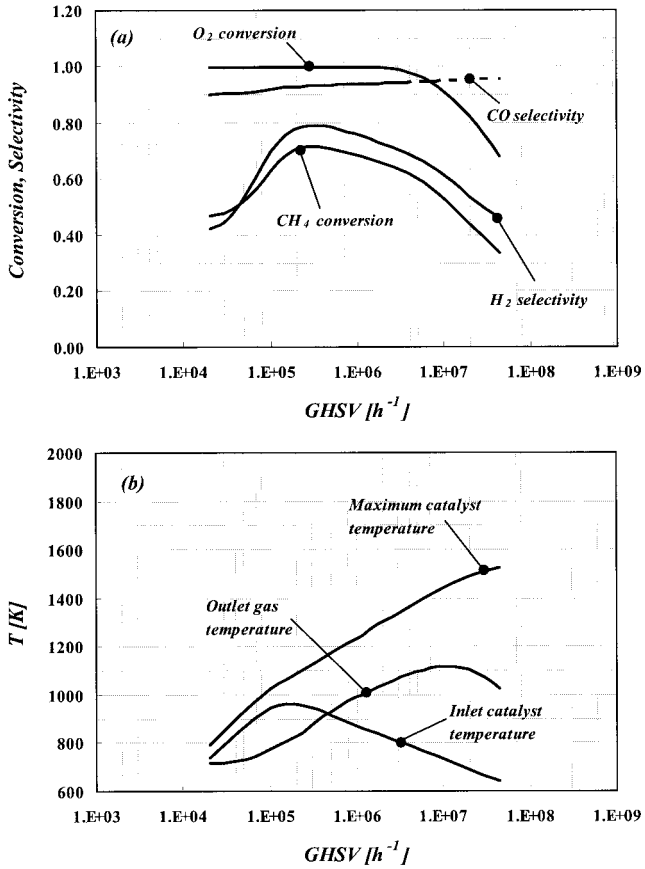

Figure 6. Model simulations at high space velocity reproducing the reactor blowout: (a) conversion and selectivity; (b) system temperatures.

sented here. However, at very high temperatures and in the presence of unconverted O_2, the gas-phase reactions neglected here could become significant. The gas-phase oxidation of CO to CO_2 near blowout conditions could therefore lead to a decline in CO selectivity, giving an expected decreasing trend at very high GHSV. For this reason, the related model predictions are reported in Figure 6 with a dashed line.

Although methane conversion decreases, the overall reacted mass flow rate of methane increases with GHSV, being the product of inlet mass flow rate and conversion. This effect produces an increasing trend in the maximum catalyst temperature curve vs. space velocity [Figure 6b]. This curve shows a possible problem that may arise in the operation at very high GHSV. If the catalyst reaches values as high as 1300 K for long periods, sintering is likely to occur and this would prevent the normal operation of the reactor. Considering the other curves reported in the same plot, it is noticed that the catalyst temperature at the fixed-bed inlet exhibits a maximum in the range between 10^5 and 10^6 h^{-1}. The maximum occurs as the increased feedstock mass flow rate forces the temperature peak to move downstream. It is noteworthy to observe that a similar curve of inlet catalyst temperature vs. GHSV was reported in Hohn and Schmidt (2001). The temperature measurements in fixed-bed reactors by means of thermocouples are known to constitute a very challenging task, and remarkable errors could occur. However, the measurements presented by Hohn and Schmidt (2001) suggest the presence of a maximum at about 10^5 h^{-1}, which is in fair agreement with our calculated result.

The outlet gas temperature has a peak in the region of high GHSV at about 1×10^7 h^{-1}. From this space velocity upward, the convection of the cold feedstock prevails over the system temperature's overall increase, and the outlet gas-phase temperature declines.

Finally, it has to be pointed out that the increase of the gas-phase temperature over values of 1200–1300 K would make the occurrence of gas-phase reactions increasingly important. In this sense the model calculations under these conditions have to be considered with much caution.

Figure 7 reports the products yields vs. space velocity. This picture confirms that the mass flow rate of converted methane increases with GHSV. Obviously the mass flow rate of unconverted methane also increases and thus the corresponding curves have an intersection at about GHSV $= 2 \times 10^7$ h^{-1},

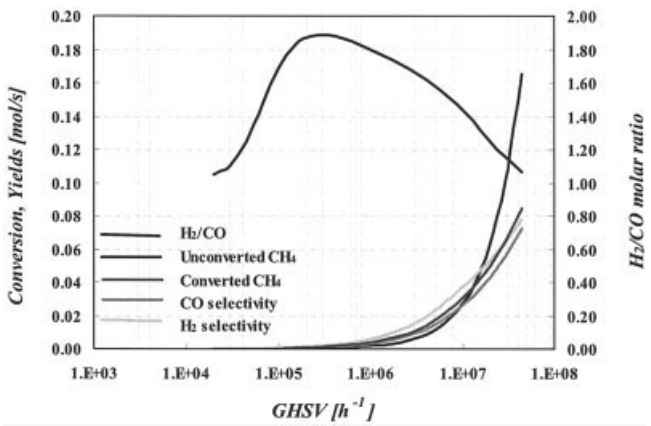

Figure 7. Product yields vs. space velocity.

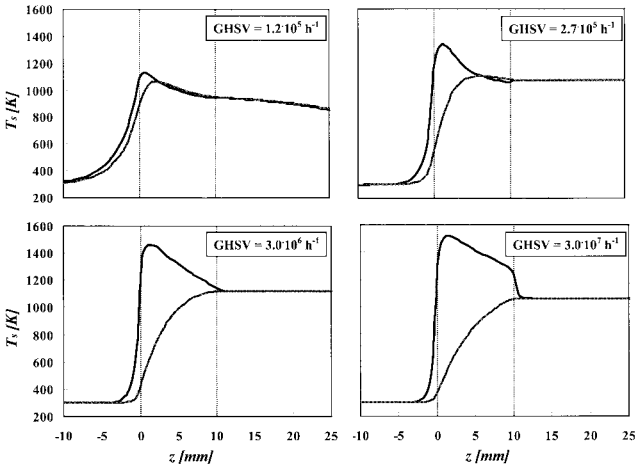

Figure 8. Model calculations of thermal profiles in the solid phase (black line) and in the gas phase (gray line).

where conversion is 50%. The product yields continuously increase with GHSV: obviously, at higher GHSV the pressure drop would increase and an increasingly higher fraction of unconverted methane would be present in the product stream, which eventually will become unacceptable. However, the results summarized in Figure 7 simply indicate that the increase in GHSV does not disturb the syngas yield. Finally, if H_2 production is desired, the optimal GHSV value would be around 200,000–300,000 h^{-1}, where the H_2/CO ratio has a maximum.

The reactor behavior near blowout can be further enlightened by considering Figure 8, which represents the calculated thermal profiles of the gas and solid phases at four different space velocities. All these graphs show a typical beneficial feature of transfer-limited systems, consisting in a considerable temperature difference between the solid and the gaseous fluid, which provides the necessary driving force for the release of the reaction energy from the catalyst surface to the gas phase. The temperature difference decreases to zero as the exothermic reactions are completed. Afterward, the occurrence of the endothermic reforming reactions entails that the gas becomes slightly hotter than the surface.

At low GHSV, the catalyst temperature peak is close to the reactor inlet [Figure 8a]. Then, the increase in GHSV determines a shift of the peak in the downstream direction. The increment in space velocity also determines an increase in the input energy entering the solid phase, thus producing higher thermal profiles of the catalyst and higher peaks. Moreover, the point at which the gas-phase temperature reaches the solid-phase temperature ($T_s = T_g$) moves downstream [Figure 8b]. With a further increment in the feedstock flow rate, the residence time becomes insufficient for the completion of the oxidation reactions—the point at which $T_s = T_g$ thus moves to the reactor outlet [Figure 8c]. This effect explains the change of slope in the CH_4 conversion curve in Figure 6a, at about GHSV $= 3 \times 10^6$ h^{-1}. From this space velocity upward, the convection of the cold feedstock prevails over the overall increase of system temperatures [Figure 8d], and the outlet gas-phase temperature declines. However, as previously noticed, homogeneous reactions could be important in this range

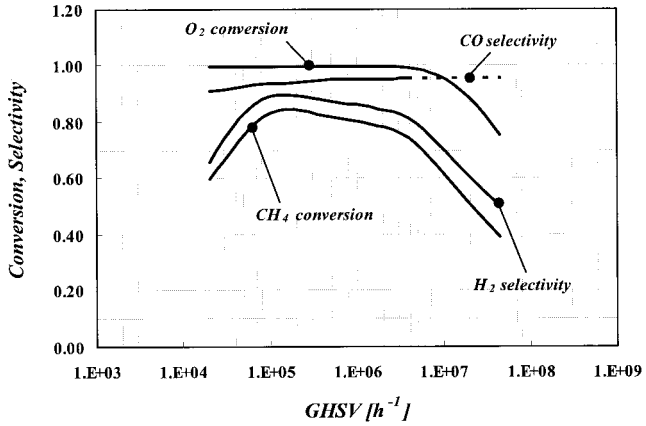

Figure 9. Model simulations at high space velocity reproducing the reactor blowout, using oxygen instead of air as oxidant (conversion and selectivity).

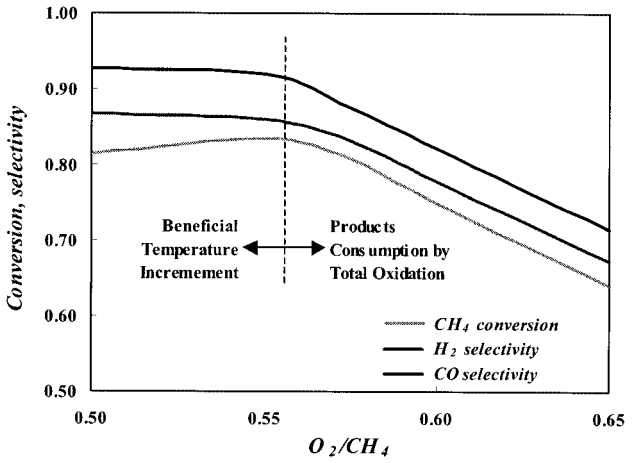

Figure 11. Effect of the O_2/CH_4 ratio on the reactor performance (GHSV = 3 × 10^5 h^{-1}).

of GHSV and above 1100–1200 K, especially because of the unconverted O_2, determining a gas-phase temperature increase.

The calculations in Figure 6 were repeated with pure oxygen instead of air (Figure 9). Figure 9 confirms that the system performance can be improved by eliminating the inert nitrogen from the feedstock. This conclusion is further developed in the following paragraph.

Effect of the feedstock composition and temperature

Figure 10 represents the variation of conversion, selectivity, and temperature with nitrogen content in the feedstock. It can be noticed that the use of pure oxygen could permit a significant improvement in performance, in terms of conversion and selectivity, because the catalyst remains at higher temperatures, thus promoting syngas formation both kinetically and thermodynamically.

The use of pure oxygen as an oxidant would determine a considerable cost of the feedstock, whereas the use of air would eliminate this cost. However, the use of nitrogen would require the compression of a considerable mass flow rate of inert gas that moreover remains in the products' stream, which could be unacceptable in certain applications. Therefore, the use of either air or oxygen could both be feasible, and considerations should be made on a case-by-case basis in industrial applications.

Figure 11 shows the dependency of the reactor performance on the O_2/CH_4 ratio in the feedstock. Methane conversion slightly improves by increasing O_2/CH_4 from 0.5 to 0.55, and then decreases. As the oxygen content of the feedstock is increased, the total oxidation reactions become increasingly favored. When the O_2/CH_4 ratio is <0.55, this effect slightly increases the system temperature, thus promoting synthesis gas production. However, at higher O_2/CH_4 ratios this beneficial effect vanishes because the total oxidation reactions prevail. This determines a reduction of the methane conversion, attributed to the total oxidation stoichiometry CH_4:O_2 = 1:2 instead of 2:1, as in the partial oxidation, and moreover the oxidation reactions start to consume the products, thus decreasing H_2 and CO selectivity.

For the sake of completeness, Figure 12 reports the system performance vs. the feedstock temperature. As previously observed, the increase of the gas-phase temperature could make the occurrence of gas phase reactions increasingly important and the calculations under these conditions have to be considered with much caution. The results show that the overall performance is obviously favored by an increase in the feedstock temperature. Because of the very short contact times of the process, the enhanced feedstock enthalpy is not completely converted into higher catalyst temperature, thus reducing the impact of this operating variable. However, the results clearly highlight that any practical method to increase the system temperature would result in improved conversion and selectivity. Nevertheless, other factors should also be considered and a considerable feedstock preheating could be nonviable, say, for safety reasons.

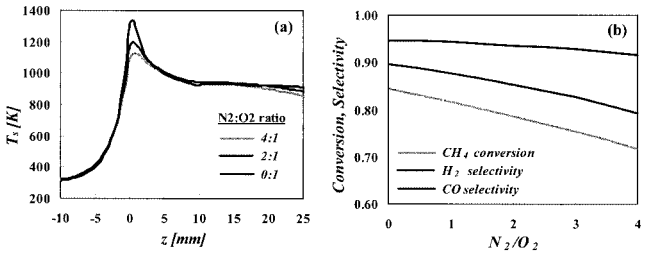

Figure 10. Effect of dilution on the reactor performance, observed by varying the N_2/O_2 ratio in the feedstock (GHSV = 3 × 10^5 h^{-1}).

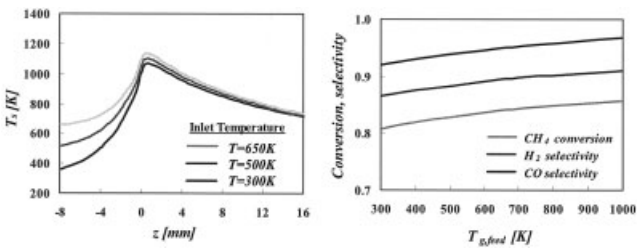

Figure 12. Effect of the gas feedstock preheating on the reactor performance (GHSV = 2 × 10^5 h^{-1}).

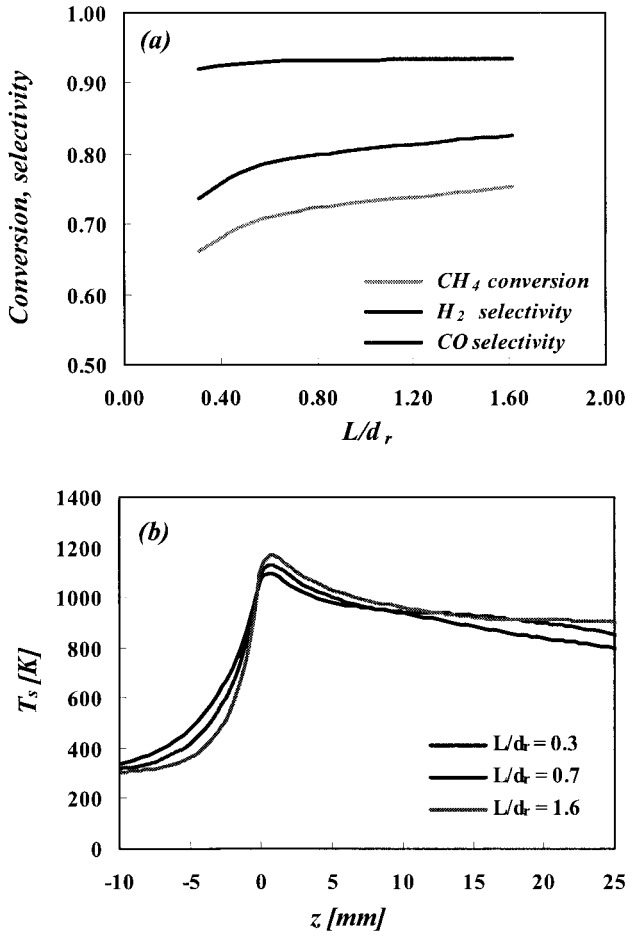

Figure 13. Influence of the reactor length to diameter ratio at constant reactor volume: (a) thermal profiles; (b) conversion and selectivity vs. GHSV.

Reactor geometry

Feedstock conversion and product yields will not be affected only by the operating conditions used, which have been discussed so far. The discussion highlighted the crucial importance of transport phenomena on the system performance. It is straightforward to notice that the transport coefficients are significantly influenced by the geometrical features of the system, which should be accordingly taken into account in the design of an industrial unit. In this perspective, simulations were carried out to show the influence of the reactor "shape" in a cylindrical configuration: the variation of conversion and selectivity was observed at different values of the reactor length to diameter ratio, at constant reactor volume. The calculations show that the system performance is improved by increasing the L/d_r ratio. Figure 13 reveals that conversion and selectivity increase with L/d_r, the thermal profiles become steeper, and the solid-phase temperature peak increases. This feature of the reactor behavior can be explained by considering that the rise in the L/d_r ratio boosts the linear velocity and the Reynolds number at constant GHSV, thus improving the transport coefficients in the reactor. Therefore the catalyst bed more effectively receives the input energy of the feedstock stream, and the thermal profiles become hotter, thus finally favoring syngas production. However, the thermal insulation could be more difficult to achieve in the case of a high L/d_r ratio and this would be an adverse factor. Moreover, as the shape factor increases, the pressure drop increases, and a trade-off condition can be found between performance improvement and increase in the required compression energy.

Reactor scale-up

The conclusions proposed on the role of the shape factor can be helpful in the study of the system scale-up. This problem is typically a challenging task for chemical engineers, and could be considered one of the fields receiving the most valuable advantages from modeling. The possibility of avoiding expensive pilot work is a considerable driving force for the development of reliable simulation tools. A precise quantitative study of scale-up, however, is beyond the scope of the present work. Scale-up of reactors was profusely considered in the past, producing a rich body of literature (Perry and Green, 1997). Nevertheless, we reported some general considerations that immediately follow the results proposed so far to highlight some reasonable guidelines on scale-up of fixed-bed reactors for short contact time, partial oxidation of natural gas.

The reactor scale-up could be carried out by maintaining a constant Reynolds number. In terms of equations, this means that the reactor volume and catalyst loading, the mass flow rate, and the cross section must be increased by the same scale factor F_{up}

$$Vol_{up} = F_{up} \tag{12}$$

$$\dot{m}_{up} = F_{up}\dot{m} \tag{13}$$

$$S_{up} = F_{up}S \tag{14}$$

By this criterion, also proposed by Hohn and Schmidt (2001), the cross section of the reactor increases with the mass flow rate, whereas the reactor depth remains unaltered. This criterion preserves the transport coefficients and therefore maintains, at the same level, the system performance as the reactor size is increased. Because the pressure drop for unit length depends on the square of the gas-phase linear velocity, which is kept constant, it could be deduced that the energy required for the compression of a unit mass flow rate of feedstock is also maintained constant.

Although this criterion is reasonable, perhaps a more rewarding strategy could be to carry out the scale-up by keeping constant the reactor shape (that is, the L/d_r ratio) as the size is increased. This may be expressed in the following equations

$$V_{up} = F_{up}V \tag{15}$$

$$\dot{m}_{up} = F_{up}\dot{m} \tag{16}$$

$$\frac{L}{d_r} = \text{constant} \tag{17}$$

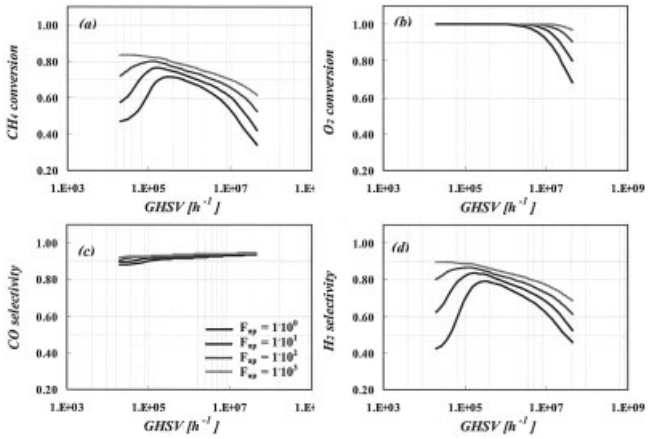

Figure 14. Reactor scale-up at constant shape factor (L/d_r): (a) CH_4 conversion; (b) O_2 conversion; (c) CO selectivity; (d) H_2 selectivity.

According to this criterion, the increase in the reactor diameter and cross section can be determined by the following relations

$$d_{r,up} = (F_{up})^{1/3} d_r \tag{18}$$

$$S_{up} = (F_{up})^{2/3} S \tag{19}$$

Correspondingly, the Reynolds number will be affected by the scale-up

$$\mathrm{Re}_{up} = (F_{up})^{1/3} \mathrm{Re} \tag{20}$$

In this case, the reactor scale-up would enhance the Reynolds number at constant GHSV and therefore the system performance would increase with size. The increased linear velocity, moreover, would force the temperature peak to move downstream and this could also be helpful in terms of process safety because it would be easier to avoid any "flashback" effect.

Figure 14 shows the results obtained by scale-up calculations with the constant geometry criterion. Methane conversion and H_2 selectivity are considerably increased as the reactor size increases, and the right-hand-side shift of the oxygen conversion curve highlights an improvement in the system stability.

Obviously, the improvement in performance takes place at the expense of an increase in the drops of reactor pressure. Together with the Reynolds number, the gas-phase linear velocity increases

$$u_{up} = (F_{up})^{1/3} u \tag{21}$$

If Darcy's law is used, then the variation in pressure drop per unit length can be calculated by the following equation

$$\left(\frac{dp}{dz}\right)_{up} = (F_{up})^{2/3} \left(\frac{dp}{dz}\right) \tag{22}$$

The different approaches for the scale-up of the reactor can therefore significantly influence the performance of the industrial unit. The criteria presented here could be considered as extremes in a real scale-up problem, and it is likely that the optimal criterion lies somewhere halfway between them. Advanced economic considerations should definitely help in finding the desired trade-off between process efficiency and costs.

Conclusions

The present article describes modeling and numerical simulation of fixed-bed reactors for partial oxidation of methane at short contact times. The model used takes into account one-dimensional two-phase energy balance, internal radiation within the fixed bed by an effective thermal conductivity, interphase heat and mass transfer, species mass balances with longitudinal dispersion, and a detailed surface reaction mechanism to represent the catalyst reactivity. The model formulated was validated against the literature data and then was used to investigate different aspects of these reactors.

The main findings of this analysis are:

- *Effect of the space velocity and reactor blowout.* At relatively low GHSV, an increment in space velocity determines an enhancement in the reactor performance attributed to better mass transfer. However, reactor blowout occurs at higher GHSV. The first reaction to be excluded by low residence times is water gas shift followed by the direct oxidation reactions.
- *Effect of the feedstock composition and temperature.* A low inert content of the feedstock favors conversion and syngas selectivity, reduces compression costs, and avoids the inert in the product stream. However, the use of pure oxygen is expensive; a trade-off condition of an optimal O_2/C ratio around 0.56 was found.
- *Reactor geometry.* The sensitivity analysis carried out on the length-to-diameter ratio at constant volume indicates that deep reactors give superior performance compared to that of wide ones at the expense of higher pressure drops; a trade-off condition was found.
- *Reactor scale-up.* Scale-up at constant Reynolds number preserves performance and pressure drop. However, the wide-shaped cylindrical reactors thus obtained could be impractical. On the other hand, a constant length-to-diameter ratio scale-up could allow a performance improvement and an increase in the required compression energy consumption; a trade-off condition was found for scale-up.

Acknowledgment

M.B. gratefully acknowledges the financial support by Prof. J. Warnatz during his stay at Heidelberg University.

Notation

A = preexponential factor of Arrhenius equation, mol, m, s
a = catalyst-specific area per unit volume, m^{-1}
$\hat{c}_p$ = specific heat, J kg^{-1}
c = molar concentration, mol cm^{-3}
d = diameter, m
D_k = diffusivity, m^2 s^{-1}
e = solid-phase emissivity
E = activation energy, J mol^{-1}
F_{up} = scale-up factor
G = superficial mass flow rate, kg s^{-1} m^{-2}
$\hat{H}$ = enthalpy of a chemical species, J g^{-1}
h = heat transfer coefficient, J K^{-1} m^{-2} s^{-1}
J = molar flux, mol m^{-2} s^{-1}
J_d = mass transfer factor

k = thermal conductivity, J s^{-1} m^{-1} K^{-1}
k_f = forward kinetic constant, mol, m, s
L = reactor length, m
m = gas-phase mass flow rate, kg s^{-1}
M = molar weight, kg mol^{-1}
N = total number of chemical species involved in the reaction environment
N_r = total number of reactions
p = pressure, atm
R = universal gas constant, J K^{-1} mol^{-1}
R_i = specific production rate of a species, mol m^{-3} s^{-1}
Re = Reynolds number
S = reactor cross-flow section, m^2
Sh = Sherwood number
t = time variable, s
T = temperature, K
u = gas-phase linear velocity, m s^{-1}
V = diffusion velocity, m s^{-1}
Vol = reactor volume, m^3
X = mole fraction
Y = mass fraction
z = reactor axial coordinate, m

Greek letters

β = Arrhenius temperature parameter
ε = porosity
κ = generic transport or kinetic coefficient, s^{-1}
ζ, ξ = surface coverage parameters
Θ = surface coverage fraction
μ = viscosity, kg m^{-1} s^{-}
ν = stoichiometric coefficient
ρ = gas-phase density, kg m^{-3}
σ = Stefan–Boltzmann constant, W m^{-2} K^{-4}
ψ = shape factor in the mass transfer coefficient equation

Subscripts

cat = catalyst
eff = effective
g = gas phase
i = generic reaction
k = generic species
kin = kinetic
in = reactor inlet
out = reactor outlet
ov = overall
p = particle
r = reactor
room = ambient conditions
s = solid phase
tr = transport
up = scaled-up reactor

Literature Cited

Beretta, A., G. Groppi, L. Majocchi, and P. Forzatti, "Potentialities and Draw-backs of the Experimental Approach to the Study of High T and High GHSV Kinetics," *Appl. Catal. A: Gen.*, **187**, 49 (1999).

Bizzi, M., L. Basini, G. Saracco, and V. Specchia, "Modelling A Transport Phenomena Limited Reactivity in Short Contact Time—Catalytic Partial Oxidation Reactors," *Chem. Eng. J.*, **90**, 97 (2002).

Bizzi, M., L. Basini, G. Saracco, and V. Specchia, "Short Contact Time Catalytic Partial Oxidation of Methane: Analysis of Transport Phenomena Effects," *Ind. Eng. Chem. Res.*, **42**, 62 (2003).

Chilton, T. H., and A. P. Colburn, "Correlating Forced Convection Heat Transfer Data and a Comparison with Fluid Friction," *Ind. Eng. Chem.*, **26**, 1183 (1934).

Deutschmann, O., *DETCHEM*, http://www.detchem.com

Deutschmann, O., and L. D. Schmidt, "Modelling the Partial Oxidation of Methane in a Short Contact Time Reactor," *AIChE J.*, **44**, 2465 (1998).

Deutschmann, O., R. Schwiedernoch, L. I. Maier, and D. Chatterjee, "Natural Gas Conversion in Monolithic Catalysts: Interaction of Chemical Reactions and Transport Phenomena," Natural Gas Conversion VI, *Studies in Surface Science and Catalysis* 136, E. Iglesia, J. J. Spivey, and T. H. Fleisch, eds., Elsevier, Amsterdam/New York, 251 (2001).

Fogler, S. H., *Elements of Chemical Reaction Engineering*, Prentice Hall, Upper Saddle River, NJ (2000).

Hindmarsh, A. C., "Odepack, a Systematized Collection of Ode Solvers," in *Scientific Computing*, R. S. Stepleman et al., eds., North-Holland, Amsterdam (1983).

Hohn, K. L., and L. D. Schmidt, "Partial Oxidation of Methane to Syngas at High Space Velocities over Rh-Coated Spheres," *Appl. Catal. A: Gen.*, **211**, 53 (2001).

Perry, R. H., and D. W. Green, *Perry's Chemical Engineers' Handbook*, 7th Edition, McGraw Hill, New York (1997).

Rostrup-Nielsen, J., "Reaction Kinetics and Scale-up of Catalytic Processes," *J. Mol. Catal. A: Chem.*, **163**, 157 (2000).

Schwiedernoch, R., S. Tischer, C. Correa, and O. Deutschmann, "Experimental and Numerical Study of the Transient Behavior of a Catalytic Partial Oxidation Monolith," *Chem. Eng. Sci.*, **58**, 633 (2003).

Yoshida, F., D. Ramaswami, and O. A. Hougen, "Temperature and Partial Pressures at the Surfaces of Catalyst Particles," *AIChE J.*, **8**, 5 (1962).

Manuscript received Feb. 24, 2003, and revision received Aug. 9, 2003.